JOURNAL OF Applied Polymer SCIENCE

Effect of Annealing Conditions on Crystallization Behavior and Mechanical Properties of NIPS Poly(vinylidene fluoride) Hollow Fiber Membranes

Jie Liu, Xiao-Long Lu, Chun-Rui Wu

State Key Laboratory of Hollow Fiber Membrane Materials and Membrane Processes, Institute of Biological and Chemical Engineering, Tianjin Polytechnic University, Tianjin 300160, China

Correspondence to: X.-L. Lu (E-mail: luxiaolong@263.net) or C.-R. Wu (E-mail: wuchunrui79@yahoo.com.cn)

ABSTRACT: In this study, a preliminary work was carried out to investigate the effect of annealing conditions on the crystallization behavior and mechanical properties of nonsolvent induced phase separation (NIPS) poly(vinylidene fluoride) (PVDF) hollow fiber membranes. The crystalline structures of surface layers and overall membranes were determined by Fourier transform infrared spectroscopy-attenuated total reflectance and X-ray diffraction, respectively. Differential scanning calorimetry and field emission scanning electron microscopy were employed to analyze the thermal behaviors and morphologies of membranes. It was found that the type of crystalline phase and degree of crystallinity of annealed membranes depended on the crystallization rate of PVDF, which in turn was determined by annealing temperature and cooling rate. For all the investigated membranes, the α and β phases coexisted in the outer surface, while PVDF mainly crystallized into α phase in the overall membrane. The percentage of α phase and degree of crystallinity increased with crystallization rate increase. The annealing process induced compaction of relatively thinner membranes; however, the pore structures did not collapse. The breaking strength of annealed membranes, associated with the variation of PVDF polymorphs and total crystallinity, was improved from 167 cN to 215 cN. © 2012 Wiley Periodicals, Inc. J. Appl. Polym. Sci. 129: 1417–1425, 2013

KEYWORDS: crystallization; membranes; properties and characterization

Received 28 June 2012; accepted 27 September 2012; published online 12 December 2012
DOI: 10.1002/app.38845

INTRODUCTION

Poly(vinylidene fluoride) (PVDF) as a semi-crystalline polymer, exhibiting outstanding properties such as chemical resistance, thermal stability, and high hydrophobicity, is quite suitable for manufacture of membrane for various membrane processes.[1–6] PVDF exhibits a well-known polymorphism depending on crystallization conditions. PVDF chains can crystallize into at least four distinct conformations, known as α, β, γ, and δ.[7–9] The most common polymorph is nonpolar α phase, which may be obtained after supercooling or quenching.[10] The polar β phase is normally obtained by drawing of α phase films or crystallizing from dimethylformamide (DMF) or dimethylacetamide(DMAc) solutions below 70°C. The two phases differ a lot in structure: the nonpolar α phase has a chain conformation of trans-gauche (TG^+TG^-), while the polar β phase has an all trans-planar zigzag conformation (TTT).[11,12] Conversion between the distinct PVDF phases may occur by convenient thermal or mechanical treatments.

The mechanical properties of PVDF may be improved through annealing process. Mohajir and Heymans[13] studied the effect of thermo-mechanical history on the structure and mechanical behaviors of PVDF, they found that an annealing temperature below the upper glass transition temperature T_{gU} (between 30 and 60°C) affected the amorphous–crystalline interphase, while a higher annealing temperature affected the crystalline phase. Therefore, mechanical properties of PVDF depended on the annealing temperatures, and furthermore, could be improved by the use of appropriate annealing treatments.[14] The cooling rate in annealing process was another important factor to influence the crystallization kinetics of PVDF, as observed by Nakagawa and Ishida[15] and Roussel et al.[16]

Generally, strength is one of the key factors that influence the application of PVDF hollow fiber membranes. In addition, the crystalline structure and total crystallinity of PVDF are very important in determining the mechanical properties of membranes as reported by Liu et al.[17] Therefore, in recent years lots of investigations have been conducted regarding the factors that affect the crystalline phase structure of PVDF hollow fiber membranes,[18–28] and a plenty of valuable results about the relationship between fabrication conditions and PVDF polymorph

Additional Supporting Information may be found in the online version of this article.

© 2012 Wiley Periodicals, Inc.

Table I. Structural Parameters of PVDF Hollow Fiber Membranes

Inner diameter (μm)	Wall thickness (μm)	Maximum pore size (μm)	Porosity (%)
850	180	0.150	86

have been obtained. However, the influences of annealing conditions on crystallization behavior and mechanical properties of PVDF hollow fiber membranes have seldom been reported and little is known on how to control the crystalline phase structure of PVDF hollow fiber membranes through convenient choice of annealing conditions.

In this work, the influences of annealing temperature and cooling rate on the formation of both α and β phases, total crystallinity, and mechanical properties of nonsolvent induced phase separation (NIPS) PVDF hollow fiber membranes were studied. PVDF hollow fiber membranes with higher mechanical properties were obtained through annealing process.

EXPERIMENTAL

Materials

The PVDF resin used is SOLEF 6010 from Solvay Solexis Company (French), which has a melt flow index of 6 g/10 min (230°C, 5 kg). The crystallizing point and melting temperature of the as-received resin are 138 and 173°C according to the product introduction. Industrial grade DMAc is used as solvent without further purification, and it is purchased from Samsung Company (South Korea).

Preparation of Samples

A mixture of PVDF/DMAc/PG (16/62/22 wt %) was dissolved in a glass flask at 70°C, followed by stirring until the solution became homogeneous. PG is a self-made additive, which favors the demixing process, and the nonsolvent used for the preparation of PVDF samples is water. The dope solution was then transferred into a tank, kept at a constant temperature of 70°C for 6 h to eliminate the air bubbles in the solution before used. Finally, the PVDF hollow fiber membranes were prepared by NIPS method using a tube-in orifice spinneret.[29,30] The casting solution and bore fluid passed through the orifice and inner tube, respectively. The bore fluid and coagulant bath were both ultrafiltration (UF) water at temperature of 70 and 50°C, respectively. The nascent membranes were taken up at a drawing rate of 25 m/min and immersed in UF water for at least 48 h to remove the residual DMAc, then kept in glycerol aqueous solution with specific gravity at 1.08 for 48 h to prevent the collapse of porous structures. Finally, the membranes were dried in ambient air until ready to use. Detailed information about the structural parameters of PVDF hollow fiber membranes was summarized in Table I.

In this work, the membranes were firstly pretreated by glycerin at room temperature to wet and protect the membrane pore structures, then the PVDF hollow fiber membranes were immersed in glycerin bath at different annealing temperatures (135, 140, 150, and 171°C) for 7.5 h, finally cooled at different cooling rates (0.3, 1.3, and 2.5 °C/min in glycerin bath). These temperatures were chosen for their position in relation to the crystallizing point (138°C) and melting temperature (173°C), thus, the recrystallization of imperfect crystalline structure was able to occur and reaching the melting temperature of PVDF resin was avoided.

Fourier Transform Infrared Spectroscopy Analysis

Infrared spectra collected directly from the outer membrane surface were obtained using a FTIR spectrophotometer (Bruker Tensor37, Germany) in the attenuated total reflection (ATR) mode. The penetration depth is typically less than one micron and thus the ATR spectra give a good representation of the skin of the membrane. From the infrared spectra of samples in the wavenumber range between 700 and 1500 cm^{-1}, the crystalline phase of PVDF can be verified. The α and β phases of PVDF are associated with the vibration band peaks at 764 and 840 cm^{-1}, respectively.[31–33]

The degree of crystallinity of α and β phases in the surface of membrane can be determined by comparing the absorbance of vibration band peaks of the samples at 764 and 840 cm^{-1}, based on the Beer–Lambert law.

$$A_\alpha = \log \frac{I_\alpha^0}{I_\alpha} = K_\alpha C_\alpha X_\alpha L \quad (1)$$

$$A_\beta = \log \frac{I_\beta^0}{I_\beta} = K_\beta C_\beta X_\beta L \quad (2)$$

where, A_α and A_β are the absorbencies, I^0 and I are the incident and transmitted optical intensities, respectively. K is the absorptivity at the respective wavenumber, and X is the crystallinity of each phase. The values of K_α and K_β are equal to 6.1×10^4 and 7.7×10^4 cm^2/mol. C_α and C_β are calculated from the densities of the two phases, resulting in the values of 0.0301 and 0.0308 mol/cm^3, respectively.[34]

X-ray Diffraction

Crystalline structures of the overall membranes were investigated through an X-ray Diffractometer (Bruker D8 advance, Germany), using Cu K α radiation at a voltage of 40 kV and a current of 40 mA. Intensities were measured in the range $10° < 2\theta < 45°$, typically with step scans of 0.05°. The characteristic diffraction peak of α and β phases were at 2θ (17.8, 18.3, 19.9, and 26.7°) and 2θ (20.6°), respectively.[19]

Differential Scanning Calorimeter

The melting temperature and crystallinity of PVDF (original membrane and annealed membranes) were characterized by a differential scanning calorimeter (Perkin–Elmer DSC-7, Wellesley, MA). The heating rate was set to 10 °C/min.

The PVDF crystallinity X_c was calculated by[35]:

$$X_c = \frac{\Delta H_f}{\Delta H_f^*} \times 100\% \quad (3)$$

where ΔH_f^* =104.7 J/g, is the melting enthalpy for a 100% crystalline PVDF, ΔH_f is the melting enthalpy of the PVDF membranes measured in DSC.

Morphology of Membranes

The cross-sectional morphology of membranes were observed by a field emission scanning electron microscope (FESEM, Hitachi S-4800, Japan) using an acceleration voltage of 5 kV. Cross-sections were prepared by fracturing the membranes in liquid nitrogen, then sputtered with gold under vacuum.

Structural Parameters of Membrane

The membrane inner diameter and wall thickness were determined by a digital microscope (Carl Zeiss Imager.A1m, Germany).

Membrane maximum pore size was determined by means of bubble point pressure, and was calculated through the formula[36]:

$$r_{\max} = \frac{C\gamma}{2P} \tag{4}$$

where C is a constant, 2860 when P is in Pa, γ is surface tension, mN/m.

The overall porosity, ε, of the membranes was calculated according to the equation:

$$\varepsilon = \frac{(W_w - W_d)/\rho_{H_2O}}{(W_w - W_d)/\rho_{H_2O} + W_d/\rho_p} \times 100\% \tag{5}$$

where W_w and W_d are the wet and dry weight of the membranes, respectively, $\rho_{H_2O} = 1.0$ g/cm^3, $\rho_p = 1.78$ g/cm^3.

Performance Test of Membranes

The measurements of UF water flux were carried out using a self-made UF setup, transmembrane pressure was set to 0.1 MPa and the temperature was fixed at 25°C.

Tensile strengths of the PVDF (original membrane and annealed membranes) were measured by an Electronic Single-yarn Tensile Tester (room temperature, 500 mm/min).

RESULTS AND DISCUSSION

Effect of Annealing Temperature

Figure 1 shows the FTIR-ATR spectra of the surface layer of PVDF membranes annealed at different temperatures for 7.5 h with the same cooling rate of 1.3 °C/min. The characteristic bands of α and β phases are indicated in the figure, and α/β values are summarized in Table II. All spectra show an evident prevalence of α phase. The α/β values of membrane surface increase as annealing temperature is increased from 135°C to 150°C, when the annealing temperature is 171°C, α/β value decreases.

As reported, in annealing crystallization of PVDF membranes it seemed that the resulted crystalline phase of the surface was determined by the crystallization rate.[20,37] An explanation for this phenomenon might be given considering that β phase in PVDF is thermodynamically meta-stable, however, α phase is thermodynamically more stable. When the annealing temperatures is 135 or 140°C, the crystallization rate is slow, so that the PVDF chains can relax and have sufficient time and thermal energy to form the thermodynamically meta-stable β phase. In contrast, when the crystallization rate is faster, as the membranes are annealed at 150°C, the mobility of chains is improved a lot and the degree of chains entanglement becomes lower, which inhibit the formation of β phase, consequently α/β value increases greatly. When the annealing temperature is as high as 171°C, the crystalline phase with lower crystal perfection melts, which results in a decrease in α/β value. The detailed thermodynamics and kinetics in annealing process will be investigated in the future.

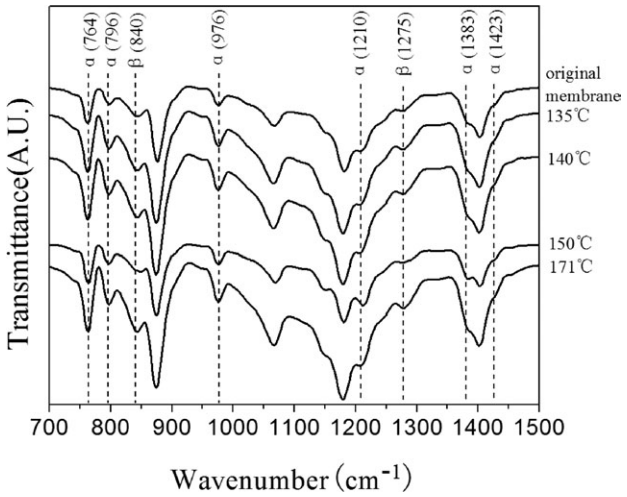

Figure 1. FTIR-ATR spectra of PVDF membranes annealed at different temperatures.

X-ray diffraction (XRD) measurements were performed to examine the crystalline phases of the overall membranes. Figure 2 shows the XRD spectra of membranes annealed at different temperatures for 7.5 h with the same cooling rate of 1.3°C/min. The results reveal that α phase is definitely predominant of PVDF crystalline with three most distinctive diffraction peaks at around 18.3°, 19.9°, and 26.7° (the membrane annealed at 171°C also has a significant diffraction peak of α phase at 17.8°). It can be clearly seen that the annealing temperature exerts an influence on the crystalline structure of the overall membrane. The membranes annealed at 135, 140, and 150°C present very similar XRD patterns (indicating that α phase portion is similar for these membranes), and have more α phase than original membrane, however, α phase decreases when the annealing temperature is 171°C.

When the annealing temperatures are 135, 140, and 150°C (near or higher than the crystallizing point 138°C), membranes undergo the re-crystallization process which induces imperfect crystalline structure to form new α phase. The decline in

Table II. Ratio of α Phase to β Phase in the Surface Layer of PVDF Membranes Annealed at Different Temperatures

Sample	α/β
Original membrane	1.30
135°C	1.34
140°C	1.40
150°C	1.62
171°C	1.29

Applied Polymer SCIENCE

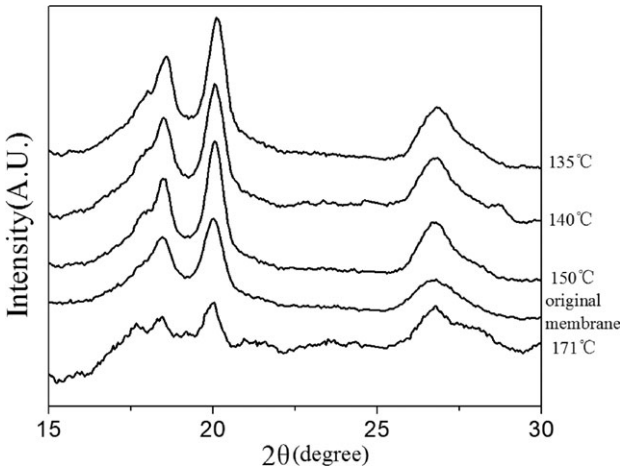

Figure 2. XRD patterns of PVDF membranes annealed at different temperatures.

characteristic diffraction peak of α phase of membranes annealed at 171°C might relate to the higher annealing temperature (near the melting temperature 173°C), as discussed above in FTIR-ATR spectra.

Thermal analysis (DSC) was carried out for all samples. Figure 3 shows typical DSC curves for PVDF original membrane and membranes annealed at 135, 140, 150, and 171°C for 7.5 h with the same cooling rate of 1.3 °C/min. The DSC measurements can give the heat of fusion (ΔH_f) and total crystallinity (X_c) of PVDF samples. The ΔH_f values are determined by peak area in the DSC curves, and these values are summarized in Table III.

In the original membrane, two endotherms are obvious with the peaks at approximately 167 and 172°C. For the membranes annealed at 135, 140, and 150°C, the same two endotherms can be observed, slightly shifted toward higher temperatures (maximum at about 168 and 174°C). This shift is predictable, since T_m increases with crystallization temperature for crystalline phase.[15,38] The peaks of the 168 and 174°C endotherms become

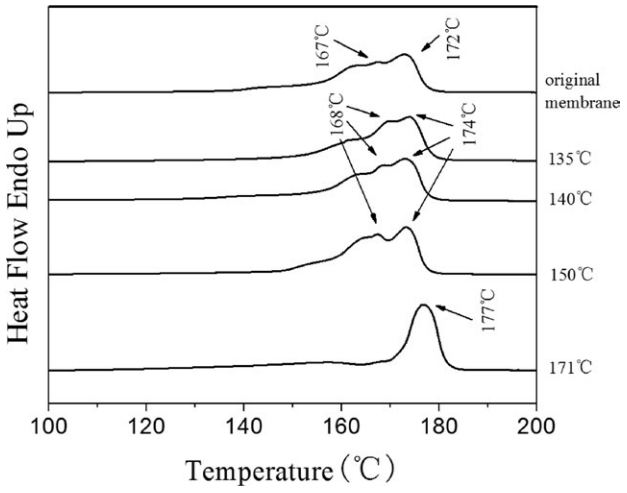

Figure 3. DSC curves of PVDF membranes annealed at different temperatures.

Table III. Effect of Annealing Temperature on Heat of Fusion (ΔH_f) and Total Crystallinity (X_c) of PVDF Membranes

Sample	ΔH_f (J/g)	X_c (%)
Original membrane	62.8	60.0
135°C	65.3	62.4
140°C	67.6	64.6
150°C	68.1	65.0
171°C	67.3	64.3

more obvious with crystallization temperature increase. The DSC curve of the membrane annealed at 171°C exhibits only one endotherm, which shifts toward higher temperature (maximum at 177°C).

A double endotherm can be usually found in the DSC curve of semicrystalline polymers. Jaffe and Wunderlich[39] and Bell et al.[40,41] had done lots of work to explain this phenomenon. One explanation is that the double endotherm is due to the melting of two different crystalline phases initially coexisting. The other is that the lower-temperature endotherm does not correspond to complete melting of a crystalline phase, but rather to melting of imperfect crystalline region or a solid-solid phase transition, and the higher-temperature endotherm is associated with melting of the crystalline phase formed by such transitions as orientation changes of crystals or re-crystallization.

PVDF crystals in different crystalline forms have different melting endotherms.[38,42,43] It had been verified that the surface layer and overall membranes had a prevalent existence of α phase based on our FTIR-ATR and XRD results. Consequently, in this case it is likely to be the level of crystal perfection rather than the different crystalline phases that determines the melting endotherms.[44] The two endotherms in the original membrane and membranes annealed at 135, 140, and 150°C present α crystalline structure with different crystal perfections. When the annealing temperatures are 135 and 140°C (near the crystalline point 138°C), the peaks of the 168 and 174°C endotherms are seen to be a little more obvious than the original membrane. In addition, the same two endotherms become much stronger at the annealing temperature of 150°C. It demonstrates that the annealing crystallization is a process in which the imperfect crystalline region can re-crystallize. When the annealing temperature is up to 171°C near the melting temperature 173°C, there is only one sharp endotherm with peak at 177°C, which is probably due to the melting of larger and well formed folded-chain crystals by re-crystallizing in annealing process. The same change can also be seen in our XRD patterns, as discussed above. The diffraction peaks of the membranes annealed at 135, 140, and 150°C are much stronger than that of the original membrane. At the same time, the membrane annealed at 171°C obtains another new significant diffraction peak of α phase at 17.8°, these results demonstrate again that the annealing crystalline is a re-crystallization process.

The X_c increases as annealing temperature is increased from 135°C to 150°C, when the annealing temperature is as high as 171°C, the X_c decreases slightly. According to DSC curve, the

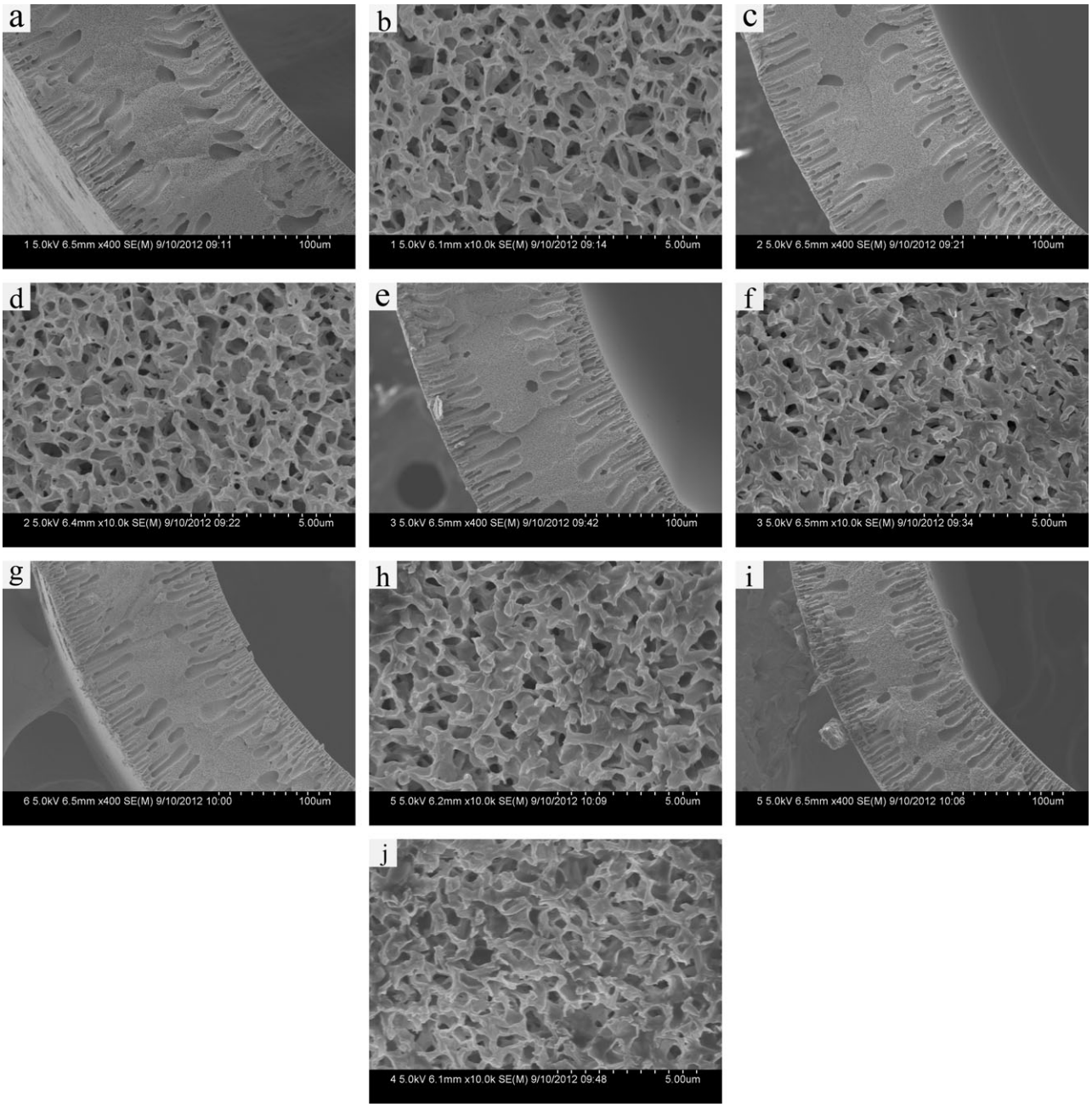

Figure 4. FESEM photomicrographs of PVDF membranes annealed at different temperatures. Cooling rate: 1.3 °C/min (a, b): original membrane; (c, d): 135°C; (e, f): 140°C; (g, h): 150°C; (i, j):171°C.

original membrane shows an endotherm over the temperature range 155–178°C, approximately. Therefore, as the membrane is annealed at 171°C, the crystalline phase partially melts, especially for some smaller crystals. When the membrane is cooled after annealing, only part of the liquid phase produced by the partial melting can crystallize in the cooling process, hence the X_c decreases slightly.[15]

Figure 4 shows the FESEM photomicrographs of the original membrane and membranes annealed at 135, 140, 150, and 171°C for 7.5 h with the same cooling rate of 1.3 °C/min. With reference to Figure 4, these membranes demonstrate relatively similar morphology with double dense skin layers, finger-like macrovoid structure near the inner and the outer surface, and sponge-like structure in the core. The double dense skin layers are formed because water is the coagulant and the bore fluid. When the annealing temperature is elevated from 135°C to 171°C, the membranes demonstrate reduced wall thickness and denser sponge-like structure. Hence, increasing the annealing temperature can make the membranes denser without destroying the original structure.

The inner diameter, wall thickness, maximum pore size and porosity of hollow fiber membrane decrease with the increase in

Applied Polymer SCIENCE

Table IV. Effect of Annealing Temperature on Structural Parameters of PVDF Membranes

Sample	Inner diameter (μm)	Wall thickness (μm)	Maximum pore size (μm)	Porosity (%)
Original membrane	850	180	0.150	86
135°C	834	171	0.131	84
140°C	818	164	0.130	83
150°C	771	150	0.124	81
171°C	670	137	0.120	71

annealing temperature as shown in Table IV. Increasing annealing temperature leads to the increase of total crystallinity that in turn promotes the compaction of PVDF molecular chains. Consequently, the membrane structure becomes denser.

The crystalline phase is generally considered to be impermeable and transport usually takes place only through the amorphous region. When crystallinity increases, the amount of amorphous phase reduces and as a result also the permeability decreases. At the same time the rubbery amorphous PVDF fraction also becomes stiffer due to the presence of the "inert" crystallites. The increase of glassy character of the amorphous phase has a negative effect on the permeability.[45]

Table V shows the effect of annealing temperature on UF flux and mechanical properties of PVDF membranes. The breaking strength of PVDF membranes increases from 167 cN to 205 cN with the increase in annealing temperature up to 150°C, when the annealing temperature is as high as 171°C, the breaking strength decreases to 193 cN. While the UF flux and the elongation at break decrease greatly with the increase in annealing temperature. The differences in the mechanical properties are directly related to the increase in total crystallinity and formation of new α phase in PVDF membranes. As discussed above, as a semi-crystalline polymer, PVDF is essentially two-phase materials. It is normally considered that crystals in the amorphous phase behave like crosslink and produce stiffening through an increase in crosslink density.[19] The predominance of α crystallites in annealed membranes contributes to improving its breaking strength compared with original membrane.

Table V. Effect of Annealing Temperature on UF Flux and Mechanical Properties of PVDF Membranes

Sample	UF flux (L m^{-2} h^{-1})	Breaking strength (cN)	Tensile stress at break (MPa)	Elongation at break (%)
Original membrane	96	167	21.9	120
135°C	83	187	22.1	107
140°C	77	195	22.9	95
150°C	65	205	25.3	87
171°C	37	193	19.5	30

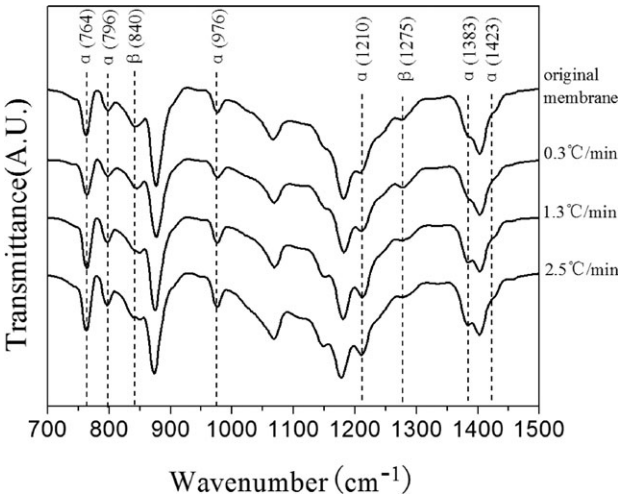

Figure 5. FTIR-ATR spectra of PVDF membranes with different cooling rates.

Table VI. Ratio of α Phase to β Phase in the Surface Layer of PVDF Membranes with Different Cooling Rates

Sample	α/β
Original membrane	1.30
0.3 °C/min	1.62
1.3 °C/min	1.62
2.5 °C/min	1.63

However, the reduction in UF flux and elongation at break is due to the increase in crystallinity and compaction of PVDF molecular chains caused by annealing process: the crystal particles become so close that they touch and interact with each other.

Effect of Cooling Rate

Figure 5 shows the FTIR-ATR spectra of PVDF membranes annealed at 150°C with three different cooling rates. The characteristic bands of α and β phases are indicated in the figure, and

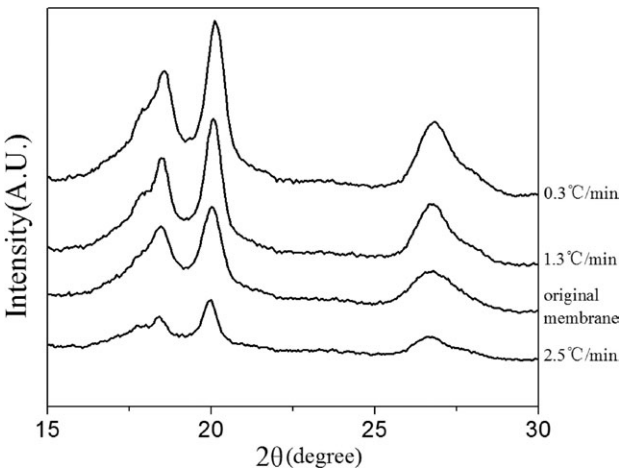

Figure 6. XRD patterns of PVDF membranes with different cooling rates.

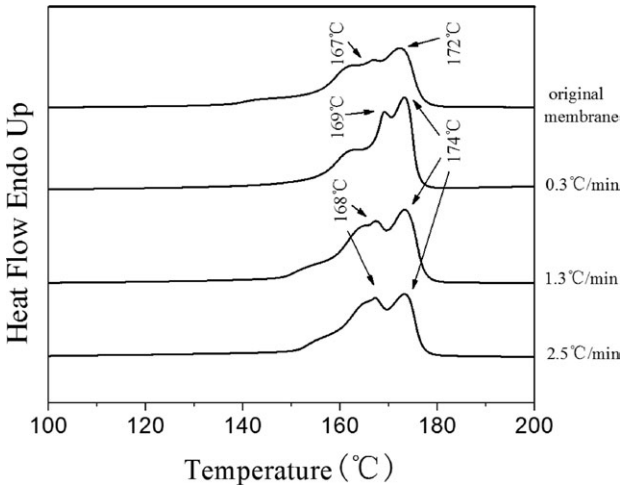

Figure 7. DSC curves of PVDF membranes with different cooling rates.

α/β values are summarized in Table VI. PVDF membranes annealed at 150°C with three different cooling rates present very similar spectra, all spectra show that cooling rate has no effect on α/β values of PVDF membrane surface.

The XRD diffraction patterns of the membranes annealed at 150°C with three different cooling rates are presented in Figure 6. It is obvious that the cooling rate also has great effect on the crystallization behavior of PVDF in the overall membrane. The characteristic diffraction peaks of α phase at 18.3°, 19.9°, and 26.7° become increasingly stronger with a decrease in cooling rate. This change suggests that the formation of α phase is preferentially under slower cooling rate, which can provide relatively longer crystalline time and higher crystalline temperature.

Table VII. Effect of Cooling Rate on Heat of Fusion (ΔH_f) and Total Crystallinity (X_c) of PVDF Membranes

Sample	ΔH_f (J/g)	X_c (%)
Original membrane	62.8	60.0
0.3 °C/min	71.3	68.1
1.3 °C/min	68.1	65.0
2.5 °C/min	59.6	56.9

Figure 7 shows typical DSC curves for PVDF membranes annealed at 150°C with three different cooling rates. The heat of fusion (ΔH_f) and total crystallinity (X_c) of PVDF samples are summarized in Table VII.

The DSC curves of membranes with three different cooling rates present very similar thermograms, they all have two endotherms with peaks at around 168 and 174°C, which become much more obvious with decreasing cooling rate. This significant change of the thermograms of membranes should be noted, demonstrating that the cooling rate exerts great influence on the level of crystal perfection, which is much higher at slower cooling rate.

The X_c increases from 56.9% to 68.1%, when the cooling rate decreases from 2.5 °C/min to 0.3 °C/min. The reason of this change can be interpreted by considering that when the cooling rate is too fast, the chains movement cannot comply with the temperature changes, so PVDF membranes crystallize at lower temperature, the PVDF chains have poor activity, the crystals grow slowly, thereby the perfection of crystalline differs a lot. When the cooling rate is 0.3 °C/min, it means there is more time for the membranes to crystallize under higher temperature, thus the X_c has been improved greatly.

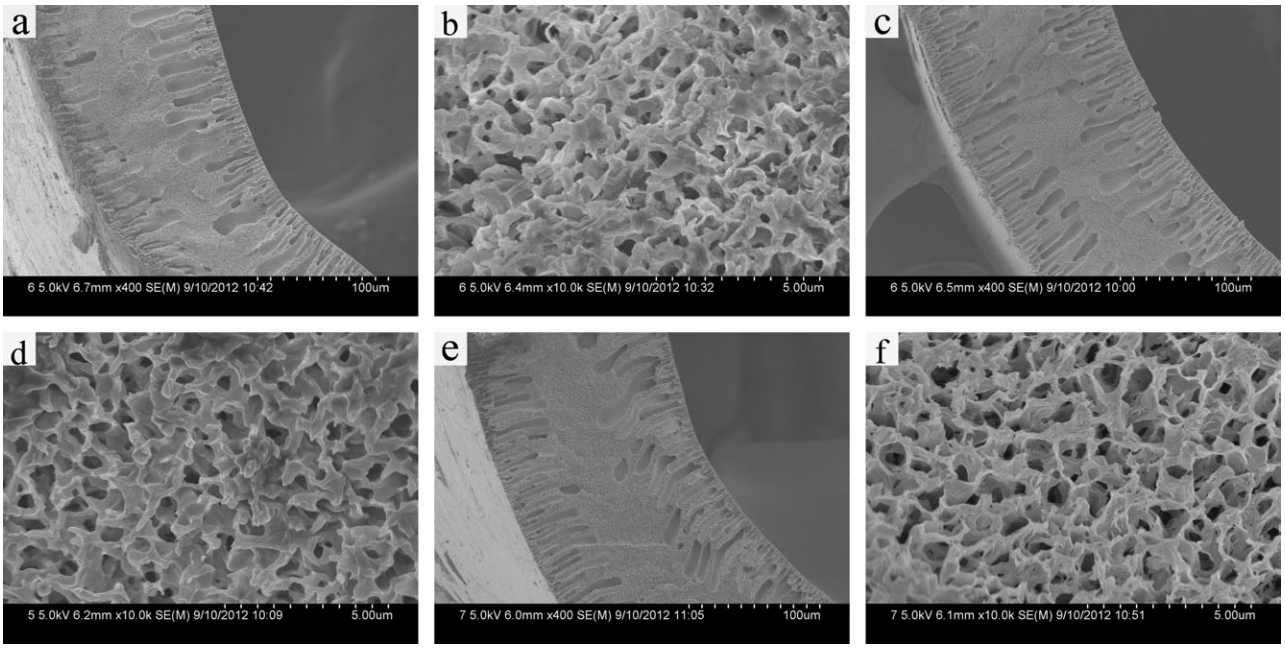

Figure 8. FESEM photomicrographs of PVDF membranes with different cooling rates. Annealing temperature: 150°C. (a, b): 0.3 °C/min; (c, d): 1.3 °C/min; (e, f): 2.5 °C/min.

Table VIII. Effect of Cooling Rate on Structural Parameters of PVDF Membranes

Sample	Inner diameter (μm)	Wall thickness (μm)	Maximum pore size (μm)	Porosity (%)
Original membrane	850	180	0.150	86
0.3 °C/min	752	141	0.121	80
1.3 °C/min	771	150	0.124	81
2.5 °C/min	781	153	0.130	82

Figure 8 shows the FESEM photomicrographs of the membranes annealed at 150°C with three different cooling rates. These membranes exhibit similar morphology, as discussed in Figure 4. When the cooling rate is slowed down from 2.5 °C/min to 0.3 °C/min, the membranes demonstrate reduced wall thickness and the sponge-like structures tend to be denser.

The inner diameter, wall thickness, maximum pore size and porosity of hollow fiber membrane decrease with decreasing the cooling rate as shown in Table VIII. Decline in cooling rate increases the time of annealing process that makes the membrane structure more compact compared with original membrane, which indicates that annealing time also has an apparent influence on the structural parameters of PVDF membranes.

Table IX shows the effect of cooling rate on UF flux and mechanical properties of PVDF membranes. When the cooling rate is slowed down, the breaking strength of PVDF membranes increases, whereas the UF flux and elongation at break decrease. These changes in the breaking strength are probably due to the increase in crystallinity of PVDF membranes, as discussed above. However, the reduction in UF flux and elongation at break is closely related to the increase in crystallinity and compaction of PVDF molecular chains caused by annealing process.

CONCLUSIONS

Annealing temperature and cooling rate are significant parameters which influence the crystallization behavior and mechanical properties of NIPS PVDF hollow fiber membranes in annealing process. For all the investigated membranes, FTIR-ATR spectra showed a mixture of α and β phases in the outer skin, while XRD measurements indicated that PVDF mainly crystallized into α phase in the overall membrane. FESEM photomicrographs of cross-sections of membranes showed that the pore structures of annealed membranes were not collapsed. The α/β of membrane surface, total crystallinity X_c, and breaking strength increased as annealing temperature was elevated up to 150°C, when the annealing temperature was as high as 171°C, these values decreased. As the annealing temperature was elevated, the values of inner diameter, wall thickness, maximum pore size, porosity, and UF flux decreased. Cooling rate had no effect on α/β of PVDF membrane surface. With the cooling rate decreased, total crystallinity X_c and breaking strength increased, while the values of inner diameter, wall thickness, maximum pore size, porosity, and UF flux decreased.

Table IX. Effect of Cooling Rate on UF Flux and Mechanical Properties of PVDF Membranes

Sample	UF flux (L m^2 h^1)	Breaking strength (cN)	Tensile stress at break (MPa)	Elongation at break (%)
Original membrane	96	167	21.9	120
0.3 °C/min	47	215	27.6	81
1.3 °C/min	65	205	25.3	87
2.5 °C/min	73	187	24.7	93

ACKNOWLEDGMENTS

This study was supported by National Natural Science Foundation of China (21176188, 21106100), Specialized Research Fund for the Doctoral Program of Higher Education of China (20111201110004), and Research Program of Application Foundation and Advanced Technology, Tianjin, China (09JCZDJC26300, 11JCYBJC04700).

REFERENCES

1. Khayet, M.; Feng, C. Y.; Khulbe, K. C.; Matsura, T. *Polymer* **2002**, *43*, 3879.
2. Khayet, M.; Matsura, T. *Ind. Eng. Chem. Res.* **2001**, *40*, 5710.
3. Bonyadi, S.; Chunorgesg, T. S. *J. Membr. Sci.* **2009**, *331*, 66.
4. Bottino, A.; Capannelli, G.; Monticelli, O.; Piaggio, P. *J. Membr. Sci.* **2000**, *166*, 23.
5. Ji, G. L.; Du, C. H.; Zhu, B. K.; Xu, Y. Y. *J. Appl. Polym. Sci.* **2007**, *105*, 1496.
6. Du, C. H.; Xu, Y. Y.; Zhu, B. K. *J. Appl. Polym. Sci.* **2007**, *106*, 1793.
7. Giannetti, E. *Polym. Int.* **2001**, *50*, 10.
8. Lovinger, A. *J. Macromolecules* **1982**, *15*, 40.
9. Kepler, R. G.; Anderson, R. A. *J. Appl. Phys.* **1978**, *49*, 4490.
10. Qudah, A. M.; Al-Raheil, I. A. *Polym. Int.* **1995**, *38*, 381.
11. Gregorio, R., Jr.; Ueno, E. M. *J. Mater. Sci.* **1999**, *34*, 4489.
12. Kobayashi, M.; Tashiro, K.; Tadokoro, H. *Macromolecules* **1975**, *8*, 158.
13. Mohajir, B. E. E.; Heymans, N. *Polymer* **2001**, *42*, 5661.
14. Mohajir, B. E. E.; Heymans, N. *Polymer* **2001**, *42*, 7017.
15. Nakagawa, K.; Ishida, Y. *J. Polym. Sci: Polym Phys. Ed.* **1973**, *11*, 2153.
16. Roussel, S.; Mcelroy, K. L.; Judovits, L. H. *Polym. Eng. Sci.* **1992**, *32*, 1300.
17. Liu, F.; Hashim, N. A.; Liu, Y.; Moghareh Abed, M. R.; Li, K. *J. Membr. Sci.* **2011**, *375*, 1.
18. Wang, Y.; Cakmak, M.; White, J. L. *J. Appl. Polym. Sci.* **1985**, *30*, 2615.
19. Buonomenna, M. G.; Macchi, P.; Davoli, M.; Drioli, E. *Eur. Polym. J.* **2007**, *43*, 1557.

20. Zhang, M.; Zhang, A. Q.; Zhu, B. K.; Du, C. H.; Xu, Y. Y. *J. Membr. Sci.* **2008**, *319*, 169.
21. Du, C. H.; Zhu, B. K.; Xu, Y. Y. *J. Appl. Polym. Sci.* **2007**, *104*, 2254.
22. Cheng, L. P. *Macromolecules* **1999**, *32*, 6668.
23. Wang, X.; Zhang, L.; Sun, D.; An, Q.; Chen, H. *Desalination* **2009**, *236*, 170.
24. Cheng, L. P.; Young, T. H.; Fang, L.; Gau, J. *J. Polymer* **1999**, *40*, 2395.
25. Lin, D. J.; Beltsios, K.; Young, T. H.; Jeng, Y. S.; Cheng, L. P. *J. Membr. Sci.* **2006**, *274*, 64.
26. Wang, X.; Zhang, L.; An, Q.; Chen, H. *J. Macromol. Sci. Part B: Phys.* **2009**, *48*, 696.
27. Vijayakumar, R. P.; Khakhar, D. V.; Misra, A. *J. Appl. Polym. Sci.* **2010**, *117*, 3491.
28. Ozkazanc, E.; Guney, H. Y. *J. Appl. Polym. Sci.* **2009**, *112*, 2482.
29. Ma, C. Y.; Huang, J. P.; Xi, D. L. *Water Sci. Technol.* **2012**, *65*, 1041.
30. Wang, K. Y.; Chung, T. S.; Gryta, M. *Chem. Eng. Sci.* **2008**, *63*, 2587.
31. Matsushige, K.; Nagata, K.; Imada, S.; Takemura, T. *Polymer* **1980**, *21*, 1391.
32. Grubb, D. T.; Choi, K. W. *J. Appl. Phys.* **1981**, *52*, 5908.
33. Salimi, A.; Yousefi, A. A. *Polym. Test.* **2003**, *22*, 699.
34. Gregorio, R., Jr.; Nocit, N. C. P. S. *J. Phys. D: Appl. Phys.* **1995**, *28*, 432.
35. Gu, M. H.; Zhang, J.; Wang, X. L.; Ma, W. Z. *J. Appl. Polym. Sci.* **2006**, *102*, 3714.
36. Lu, X. L. *Membr. Sci. Technol.* **2011**, *31*, 1.
37. Gregorio, R., Jr.; Borges, D. S. *Polymer* **2008**, *49*, 4009.
38. Gregorio, R., Jr.; Capitao, R. C. *J. Mater. Sci.* **2000**, *35*, 299.
39. Jaffe, M.; Wunderlich, B.; Kolloid Z. *Z. Polym.* **1967**, *203*, 216.
40. Bell, J. P.; Slade, P. E.; Dumbleton, J. H. *J. Polym. Sci.* **1968**, *1773*, 6.
41. Bell, J. P.; Dumbleton, J. H. *J. Polym. Sci.* **1969**, *1033*, 7.
42. Gregorio, R., Jr. *J. Appl. Polym. Sci.* **2006**, *100*, 3272.
43. Gregorio, R., Jr.; Cestari, M. *J. Polym. Sci. Part B: Polym. Phys.* **1994**, *32*, 859.
44. Prest, W. M., Jr.; Luca, D. J. *J. Appl. Phys.* **1975**, *46*, 4136.
45. Choi, S. H.; Tasselli, F.; Jansen J. C.; Barbieri, G.; Drioli, E. *Eur. Polym. J.* **2010**, *46*, 1713.